Graefe's Arch Clin Exp Ophthalmol (1999)
237:1014–1023

CLINICAL INVESTIGATION

Johann Sjöstrand
Zoran Popovic
Nils Conradi
John Marshall

Morphometric study of the displacement of retinal ganglion cells subserving cones within the human fovea

Received: 4 May 1999
Revised version received: 2 September 1999
Accepted: 22 September 1999

J. Sjöstran (✉) · Z. Popovic
Institute of Clinical Neuroscience,
Department of Ophtalmology,
SU Mölndal, SE-43180 Mölndal, Sweden
e-mail: johan.sjostrand@oft.gu.se
Fax: +46-31-412904

N. Conradi
Department of Pathology,
University of Göteborg, Sweden

J. Marshall
Department of Ophtalmology,
St. Thomas' Hospital, London, UK

Abstract ● Background: A study was carried out to measure the displacement of retinal ganglion cells subserving the cones within the human fovea. ● Methods: Four human retinas were examined along the nasal or vertical hemi-meridians. Total displacement was estimated by adding the displacement due to fibres of Henle and bipolar cells, measured as the lateral extension of the Henle fibres and of the obliquely running fibre bundles within the inner nuclear layer, respectively. ● Results: At the foveal border (0.5–0.8 mm or 1.8–2.9 deg eccentricity) the mean offset due to fibres of Henle and mean total lateral displacement was at a maximum of 0.32±0.03 mm and 0.37±0.03 mm, respectively. A steep decrease of displacement was found outside the foveal border out to an eccentricity of 2.0–2.5 mm. We were able to plot displacement along the vertical meridian in relation to eccentricity with good correlation between three eyes. The data were used to establish different mathematical functions describing the relation between eccentricity and displacement. These functions were applied to previously presented data on densities of retinal ganglion cells and cones. ● Conclusions: The present estimates of displacement within the human central fovea offer the possibility of analysis of quantitative relations between cones and retinal ganglion cells. Our data provide predictive guidance by establishing that vitreo-retinal procedures causing damage to retinal ganglion cells up to 1 mm from the foveal centre could have implications for loss of information generated within the fovea.

Introduction

The centralmost area in the human adult fovea, the foveola (diameter about 300–400 µm or 1.1–1.4 deg), contains no retinal ganglion cells (RGC). Outside the foveola the fovea increases in thickness and the number of layers of RGC steeply increases to a maximum at the foveal border (diameter of the fovea approximately 1.4 mm or 5.0 deg [18]). In the fovea, the inner connecting fibres of cones, Henle fibres, run centrifugally from the cone soma to the cone synapse, the pedicle. However, detailed knowledge of the cell displacement within the complex geometry of the human fovea is scarce. Direct measurements at different eccentricities of the length of the Henle fibres, from the body of the cone photoreceptors to the pedicles (for discussion, see [2, 18]), together with estimates of the distance from the image point at the level of the cone inner segments to the level of the ganglion cell dendrites in the inner retina, are largely unavailable. From developmental studies of the human and macaque retina we know that the extended fibres of Henle are formed due to a pattern of movements rearranging RGC and cones during the formation of the fovea [12, 16, 27]. The displacements between cones and RGC are formed by the centripetal movement of cone cells at the same time as development forces displace RGC away from the foveola. The inner connecting fibres of cones in the adult fovea therefore run centrifugally

from the cone nuclear region to the cone synapse, the pedicle.

In macaque monkeys careful measurements of displacement were obtained using whole-mount Golgi preparations ([14, 17]; Wässle, personal communication) and/or vertical sections [20, 24]. Wyatt [25] used such data for human retina, assuming similar displacements, and others have adjusted for differences in eye axial lengths between macaques and humans [21]. Even though there are great similarities between the macaque and human fovea the question has arisen whether and how macaque data may be extrapolated to human fovea. In previous studies of the morphology and resolution thresholds of the human fovea [6, 21] only indirect estimates of lateral displacement were presented. Sjöstrand et al. [21] calculated displacement values from differences between the cumulative numbers of cones and RGC and from assumptions about the number of RGC connecting with every cone within the fovea. Curcio and Allen [2] used a similar approach for indirect estimates.

However, directly measured human lateral displacements are needed in order to improve understanding of the connections and quantitative relationships between cones and RGC in the human fovea. The results presented by Marshall et al. [13] could offer an opportunity for direct measurement of displacement. Argon laser lesions were induced at different distances from the foveola in a human eye prior to enucleation for an anterior malignant melanoma. In cases where the cell bodies of cone photoreceptors were damaged, pyknotic changes resulted in darkly stained inner connecting fibres of cones (Henle fibres), which could be observed extending from the lesion in the pigment epithelium and overlying cones to their pedicles.

These degenerating fibres are well suited for length measurement in sections where the distance to the foveola may be measured with high accuracy. In addition, measurements of well-stained Henle fibres in aligned vertical sections of normal retinal specimens would give comparable length estimates of displacements within unlesioned areas of the fovea. Such normal human foveas were available from ongoing studies on the quantitative morphometry of the fovea [21, 22].

Developments in both the surgery of macular holes [8–10] and their imaging using optical coherence tomography [11, 19, 23] have led to a need for a further understanding of the microanatomy of this region. To evaluate the potential visual impact of foveal lesions a three-dimensional description of normal foveal topography and cellular connections is needed.

The purpose of this study was to present direct measurements of the axial offset produced by the fibres of Henle and to estimate the total displacement of RGC from cones in the human central retina. Such calculations will allow estimates of the proportion of RGC to cones serving a specific part of the visual field; in addition, the location of disconnected cones and central scotomas can be predicted when the centrifugally displaced RGC within the inner retina are damaged.

Materials and methods

Case descriptions

Material was obtained from two sources. The eye of case A (63 years of age) was enucleated due to an anterior melanoma not involving the posterior retina. This retina was irradiated with an argon laser prior to surgery, as described in a previous study [13]. Argon laser burns were delivered via a Coherent Radiation 800 clinical laser system, using a slit lamp, and the burns have the following parameters: pulse duration 200 ms, spot size 50 µm, emitted power 87 mW. Three retines of normal eyes were obtained during the course of surgery for maxillary carcinoma (case B [21], cases C and D [22]; 39, 49 and 73 years of age, respectively). There was no infiltration of the malignant tumours into the eyes. The pre-enucleation therapeutic regimes had not resulted in observable changes in morphology in any of the specimens studied. The research followed the tenets of the Declaration of Helsinki.

The laser-irradiated eye (case A) was enucleated 20 h after laser irradiation and fixed by immediate immersion in 3% glutaraldehyde (for details see [13]). The tissue was osmicated subsequent to glutaraldehyde fixation and a wash in sucrose buffer. Specimens were immersed for 1 h in 2% osmium tetroxide buffered in 0.2 M sodium cacodylate buffer. They were embedded via an ascending series of alcohol concentrations, through epoxypropane into Epon. The three normal eyes were fixed either in 3% glutaraldehyde and 3% paraformaldehyde (case B) or in 0.5% glutaraldehyde and 2% paraformaldehyde (cases C, D). Specimens from case B were embedded in Epon following osmication as described above: For cases C and D, specimens were rinsed, dehydrated in an ascending series of ethanol and infiltrated with 100% acrylic resin Unicryl overnight. The resin was then polymerized at 52°C over a maximum period of 3 days. Effects of shrinkage was controlled by comparing size of original tissue blocks with size in sections.

Measurement techniques

Displacement due to the fibres of Henle was measured from the exit of the inner cone fibre from the outer nuclear layer, containing the cone cell body, to the pedicle in 1-µm sections cut along the nasal hemi-meridian through the foveal centre (laser-irradiated soecimen) or along the vertical meridian out to 9 mm eccentricity (normal specimens). Due to the pathology of the outer nuclear layer within the laser lesions the initial portion of the cone fibre could not be traced. The distance from the centre of the foveola to the exit of the fibre of Henle from the outer nuclear layer was therefore taken as a measure of cone eccentricity. From this point, individual fibres of Henle were followed to their respective cone pedicles and the axial offset parallel to the outer limiting membrane was measured.

The tracking of Henle fibres in semithin sections was performed in the following way. Since these cone axons take a long radial course, the implication is that they are running through the layer of Henle within a thin radial slice of foveal tissue. Therefore, radially well-aligned specimens were selected the horizontal and vertical meridians in the present study. In spite of this, it is often difficult to identify and track individual cone fibres of a diameter of approximately 1–2 µm due to the fact that the fibres within a section are neither perfectly straight nor perfectly aligned at all measurement locations. In the first stage of this investigation the sampling and measurement problems were there-

fore evaluated as follows: The degenerating Henle fibres from the border of the cone lesions caused by the argon laser were studied where the degenerating fibres were well marked. In spite of good alignment within the specimen in general, fibres from some laser lesions could show obliquely sectioned axons where the degenerating Henle fibres are seen as a series of oblique profiles. Due to the thinness of the cone axon and of the section a small angular difference between the two, depending on the section angle or to some bending (described by Perry and Cowey [17] in macaque), will give rise to this phenomenon. The parameter measured in this study was the vectoral length parallel to the retinal surface instead of the true running length of the Henle fibre. The effect on the displacement measurements of this underestimation of total fibre length at some locations was therefore minor (Fig. 1d).

A second observation was that the degenerating fibres within the lesions and the well-stained cone axons outside the lesions show an orderly arrangement, like tiles on a roof, from about the border of the foveola towards periphery. Although the thickness of the layer of Henle in radical sections changes with eccentricity, the cone fibre descends at an angle that shows minor changes. During the measurement of a specific cone fibre, important information could therefore be obtained from the neighbouring ones if they were better aligned in certain areas. At the same time it was observed that several fibres outside the lesions were well stained and adequate for displacement measurements.

A third observation was that it was difficult to obtain adequate alignment of cone fibres within the foveola with more irregularities within the layer of Henle. No measurements were therefore performed in the foveola. In the specimens of the three normal cases the same general observations were made and the same sampling strategy was used. The course of a cone axon in serial sections was judged from either a complete or nearly complete axon profile or from the radial course of a sequence of oblique sectioned axon profiles. By following the course of neighbouring axons extending into the pedicle layer the final S-formed course of the cone axon could be estimated and the positioning of the pedicle indicated. When measuring displacements one further problem was apparent in the semithin sections. In most sections it was not possible to follow that short part of the cone axon which extends from the cone soma to the axon's entrance into the Henle layer. However, occasional and well-aligned and well-stained cone fibres within the outer nuclear layer were observed and used to evaluate this portion of the total displacement.

In the sections of the laser-irradiated specimen (case A, nasal hemi-meridian) and one normal specimen (case D, inferior vertical hemi-meridian) the lateral displacement within the bipolar cell layer was estimated by measuring the axial offset caused by obliquely coursing bipolar and Müller cell processes. A linear least squares fit to the displacement of bipolar cells (y) at various eccentricities (x) along the inferior vertical hemi-meridian of case D (y=–0.026·x+0.068; cf. Eq.II, Fig. 2), was also used for the other three cases with data along the vertical meridian. In our calculations, total displacement was calculated by adding the displacement due to the fibres of Henle to that within the bipolar layer. The minor degree of lateral displacement caused by the bipolar axons within the inner plexiform layer and the dendritic trees of RGC is at present unknown in humans and therefore not included in calculations of total displacement (Fig. 1d).

Shrinkage due to the dehydration process as estimated by measuring the length of specimens prior to dehydration and in sections was found to be less than 5%. This is in agreement with reports showing that total change in tissue volume during fixation and embedding in resins is negligible [5]. Hence, the present data were not compensated for this limited shrinkage.

Retinal arc lengths were converted from millimetres to degrees according to the curve for retinal eccentricity by Drasdo and Fowler [4].

Table 1 Cell densities versus eccentricity. Mean values from superior and inferior vertical hemimeridians of cases B, C and D. Data from [22]

Eccentricity		Density	
(mm)	(deg)	Cones (cells/mm^2)	RGC (cells/mm^2)
0.6	2.2	20084	43667
0.8	3.0	14599	37491
1.6	6.0	11085	19772
2.4	9.0	8134	8435
3.0	11.2	7615	7452
5.0	18.7	5995	3241
7.0	26.2	5435	3484
9.0	33.7	4998	2415

Cell density estimations

Calculations in this study based on cell densities of three (originally reported by Sjöstrand et al. [21]; see Table 1). Cells were counted using a modified disector method. The counting was made on digital images acquired at an objective magnification of ×100 (oil immersion lens) and presented in pairs on a television monitor. Nuclei were counted only if they were seen in one (reference) but not in the next (look-up) section. Nuclei touching "forbidden lines", i.e. two out of four edges of the measuring field, were excluded. The counting frame was 100 µm wide and the section thickness was 1.0 µm. Thus the area of retinal surface in each disector was 100 (counting frame width) ×1 (section thickness) µm^2 (or 10^4-mm^2). By using this modified disector the number of cells per unit of retinal surface area (N/mm^2) could be estimated. See [22] for further details.

Results

Displacement

The lesions in the human fovea caused by the argon laser (Fig. 1) were primarily characterized by damaged pigment epithelial and photoreceptor cells (see [13] for details). Darkly stained fibres of Henle extending from these lesions could be observed and easily measured from the borders of the lesion. Well-stained sections from normal retinal specimens, also in adequate alignment to the plane of cone fibres, were also used to measure displacement in unlesioned retinae.

The displacement within the layer of Henle due to the cone fibres and within the bipolar layer is presented as a scatter plot of all data (Fig. 2). The axial offset due to the fibres of Henle was maximal at the foveal border. From 0.5 to 0.8 mm eccentricity (1.8–2.9 deg) the mean offset due to the fibres of Henle along the measured hemi-meridians was 0.33±0.03 mm and the total displacement was 0.38±0.03 mm. Outside the foveal border the offset decreases steeply out to about 2–2.4 mm (7.2–8.6 deg) eccentricity along the nasal (laser-irradiated specimen) and vertical hemi-meridian (normal specimens). The gaussian squares fit (Eq. I) for the length of the fibres of

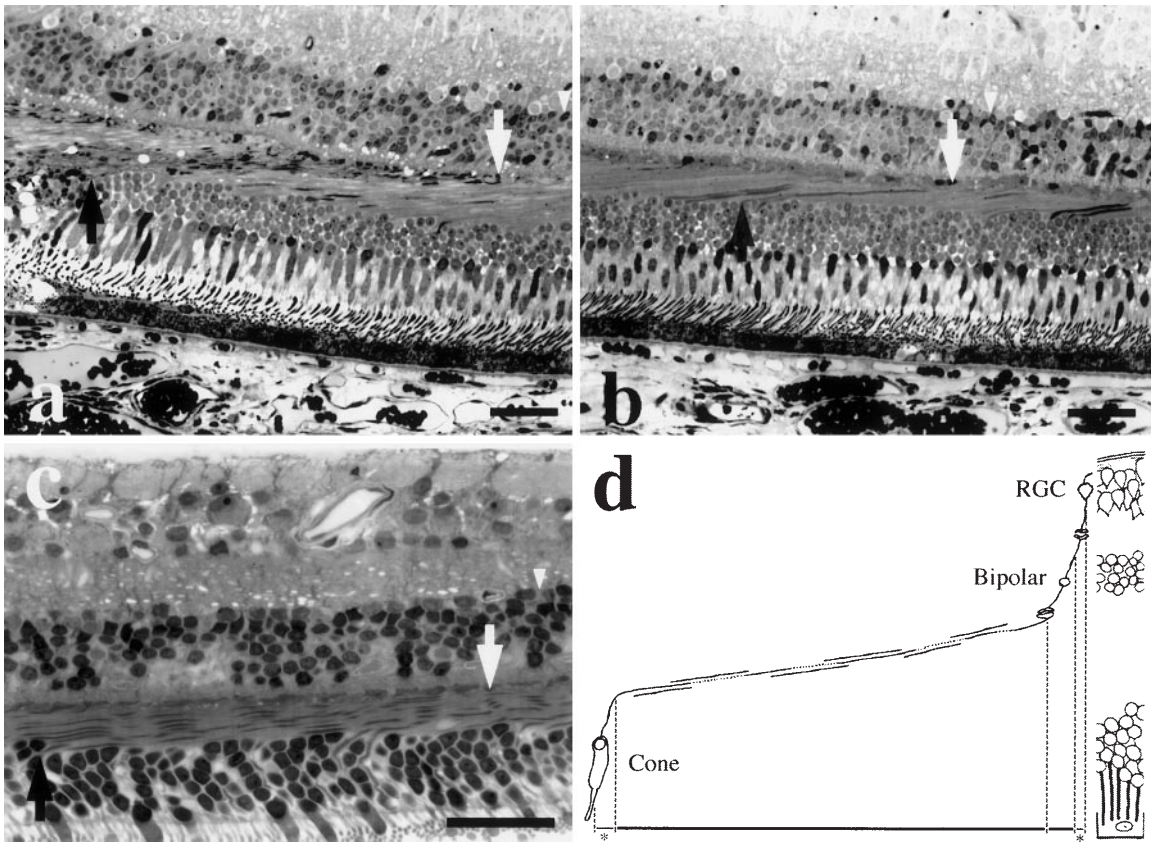

Fig. 1a–d Photomicrographs from two human foveas. Bars=50 µm. **a** Case A, nasal hemi-meridian, cone eccentricity 1.0 mm, at the rightmost border of a laser lesion. **b** Case A, nasal hemi-meridian, cone eccentricity 1.6 mm, 0.6 mm peripheral to the laser lesion in **a**. **c** Case D, vertical hemi-meridian, cone eccentricity 1.7 mm. Displacement due to fibres of Henle was measured as the axial between the point where the lesioned or unlesioned fibres exit from the receptor or outer nuclear layer (*black arrows*), defined as cone eccentricity, and the point where the fibre terminates in the pedicle (*white arrows*). Total displacement was obtained by adding the axial offset due to the oblique course of bipolars, between the pedicle (*white arrows*) and the inner limit of the bipolar cell layer (*white arrowheads*), to the displacement due to fibres of Henle. **d** A schematic showing the post-receptoral components of displacement and demonstrating how tracing was performed. The segments omitted in the displacement measurements, from the cone inner segment (image plane) to the exit from the receptor or outer nuclear layer and from the inner limit of the bipolar cell layer to the RGC, are marked with an *asterisk*

Henle (y) as a function of cone eccentricity (x) along the vertical meridian was $y=0.32\cdot\exp(-((x-0.73)/1.03)^2)$ (correlation coefficient, $r=0.93$). The radial offset due to the fibres of Henle alone, or with postreceptoral displacement within the bipolar layer added (Eq. II, Fig. 2), showed similar slopes for the different hemi-meridians (the temporal was not studied). The displacement along the nasal hemi-meridian is in the upper range of data (regression line not shown). The measured offset due to the fibres of Henle along the vertical meridian at a cone eccentricity of 3 mm (10.8 deg) was on average 0.045 mm with almost perpendicular cone connections through the retina at higher eccentricities, Figure 3 presents all data of total displacement as a function of cone eccentricity and the best least squares fit for the data along the vertical meridian (Eq. III). At the foveal wall (0.5–0.8 mm or 1.8–2.9 deg) along the vertical meridian the displacement (mean±standard error of the mean) within the layer of Henle was 0.32±0.03 mm and the total displacement was 0.37±0.03 mm.

RGC eccentricity could then be plotted as a function of cone eccentricity (Fig. 4) along the vertical hemi-meridians, where the present study derived most measurements, and the equation describing their relation was established (Eq. IV).

‘Effective’ RGC density

Mathematical models of the functional microanatomy of the human fovea are presented in Fig. 5. The calculations were based on raw RGC densities along the vertical meridian of three normal retinae [22] and those of Curcio and Allen [2], the total displacement data of the present study (Eq. IV, Fig. 4) and cone data from previous studies [3, 21, 22]. Two of the effects of lateral displacement are (1) that RGC at a certain eccentricity ac-

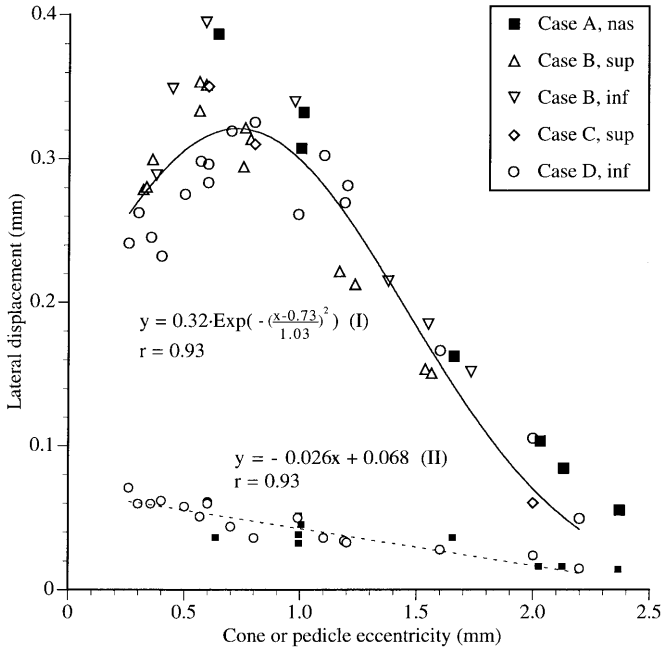

Fig. 2 Lateral displacement as a function of cone or pedicle eccentricity. The *upper* scatterplot shows radial offset due to the fibres of Henle. Data from one laser-treated human retina (case A; nasal hemi-meridian, *filled symbols*) and three normal human retinas (cases B, C and D; vertical hemi-meridians, *open symbols*) are presented. A gaussian least squares fit to the vertical hemi-meridian data is shown (Eq. I). The *lower* scatterplot shows displacement within the bipolar or inner nuclear layer as a function of pedicle eccentricity from one nasal hemi-meridian (case A) and one inferior hemi-meridian (case D) together with a linear least squares fit to the inferior hemi-meridian data (Eq. II)

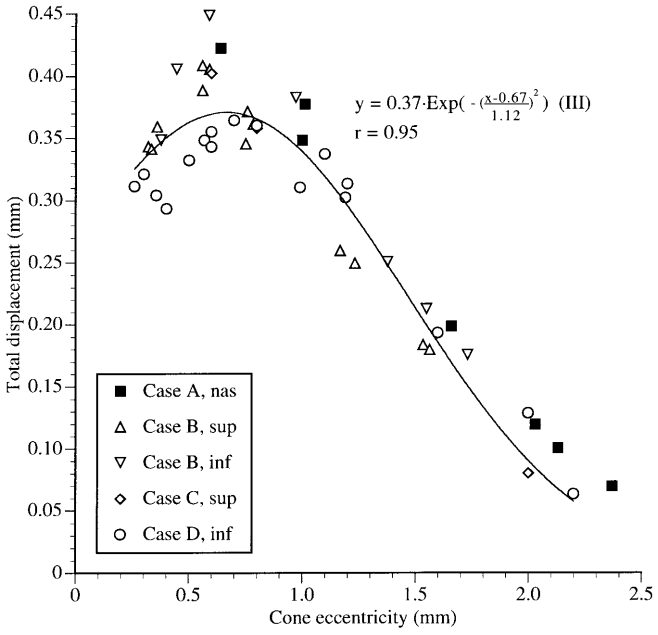

Fig. 3 Total lateral displacement (due to fibres of Henle and bipolar cells, cf. Fig. 2) as a function of cone eccentricity. Data from one laser-treated human retina (case A; nasal hemi-meridian, *filled symbols*) and three normal human retinas (cases B, C and D; vertical hemi-meridians, *open symbols*) are presented. A gaussian least squares fit to the vertical hemi-meridian data is shown (Eq. III)

tually sample the visual image from an area closer to the foveola and (2) that the area taken up by a group of RGC cell bodies is larger than that allowed for their sampling cones. By using the displacement data between RGC and corresponding cones from this study, "effective" RGC densities could be derived from raw RGC densities. In Fig. 5a, such raw and effective RGC densities as a function of eccentricity within the central human retina are compared.

RGC:C ratio and estimated receptive field

The transformation to effective RGC densities made it possible to compare the sampling characteristics of cones and RGC. Mathematically derived RGC:C ratios (Fig. 5b) were established by dividing established equations for effective RGC density [22]: $y=63\ 300\cdot(x+0.47)^{-1.73}$; [2]: $y=10\ 200\ 000\cdot(x+3.21)^{-4.10}$) with those of corresponding cones [22]: $y=10\ 920\cdot(x+0.41)^{-0.36}$;[3]: $y=17\ 300\cdot(x+0.02)^{-0.89}$). Figure 5b demonstrates that in spite of a marked difference in RGC:C ratio at the foveal border, both ratios decrease outside the fovea, presumably due to

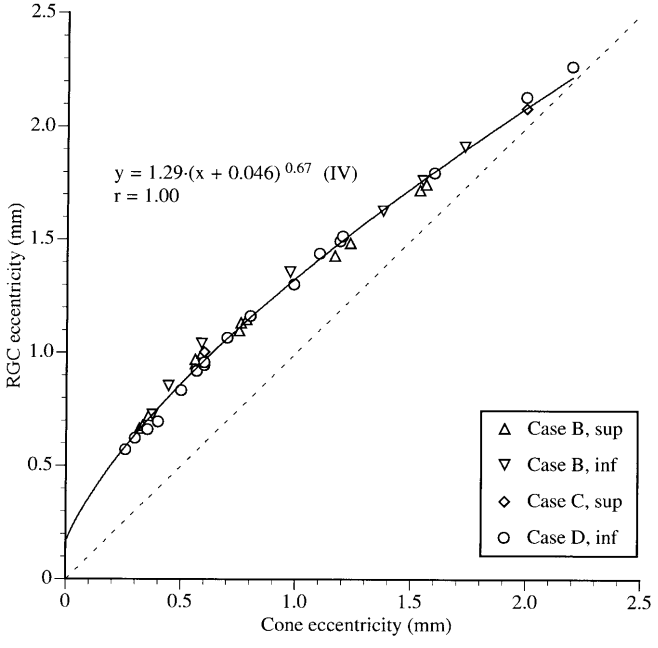

Fig. 4 RGC eccentricity as a function of cone eccentricity, for specimens of vertical hemi-meridian of three human subjects (cases B, C and D). The RGC eccentricity corresponding to a certain cone eccentricity is calculated by adding total displacement (cf. Fig. 3, Eq. III) to the cone eccentricity. A least squares curve fit to the data is presented (Eq. IV), thereby yielding a single equation relating cone and corresponding RGC eccentricity

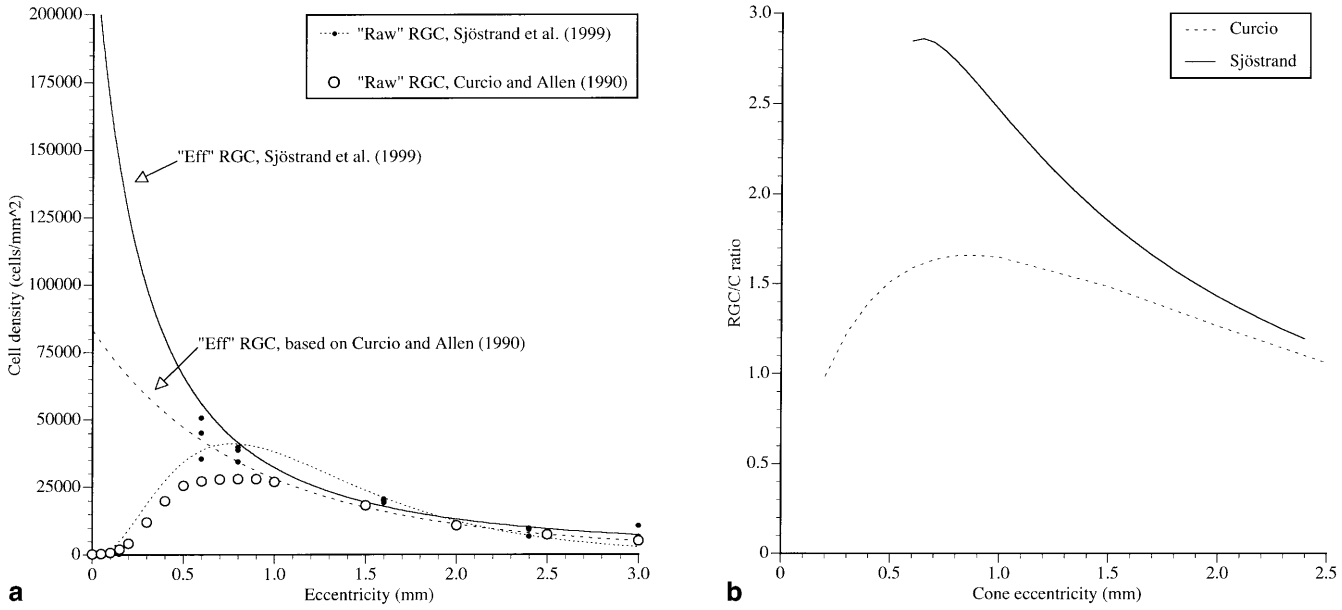

Fig. 5a, b **a** Raw RGC density (*filled circles*, *dotted line*) and calculated corresponding effective RGC density (*continuous line*) as a function of eccentricity, from [22]. As a comparison we present mean raw RGC density data (*open circles*) from [2] and calculated effective RGC density data (*interrupted line*) based on our total displacement values (Eq. III, Fig. 3). Knowing the total displacement, raw RGC densities at a certain eccentricity can be transformed to effective densities by calculating the density the RGC would have if they were placed vertically above their corresponding cones and compensated for areal magnification [20]. **b** Mathematically derived RGC:C ratios. The *continuous line* is based on RGC and cone data from [22] and the *dashed line* is based on RGC and cone data from [2] and [3], respectively. The ratios are calculated by dividing fitted effective RGC density functions (**a**) with fitted cone density functions (mean of superior and inferior hemi-meridians)

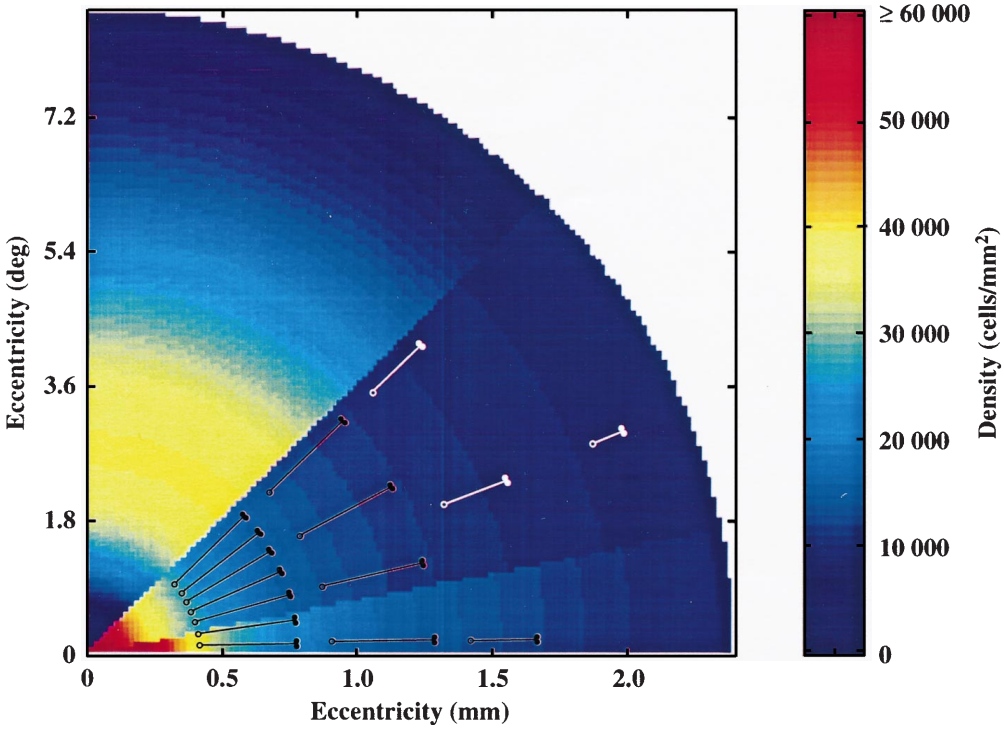

Fig. 6 Colour density distribution map along the vertical meridian (mean of superior and inferior hemi-meridians) of our raw RGC density (*top segment*, cf. Fig. 5a) and of estimated receptive field centre density (*middle segment*) and of cone density (*bottom segment*; function fitted to the data of [2], the most complete data set including the foveola available) versus eccentricity. In order to estimate the area from which one RGC receives information, i.e. the estimated receptive field, we have divided effective RGC density with the RGC:C ratio at the foveal border (cf. Fig. 5b). A number of schematic sampling units, for simplicity consisting of two RGC and one connected cone, are inlaid in the two lower segments illustrating total RGC displacement at different eccentricities (○— cones, ●— RGC)

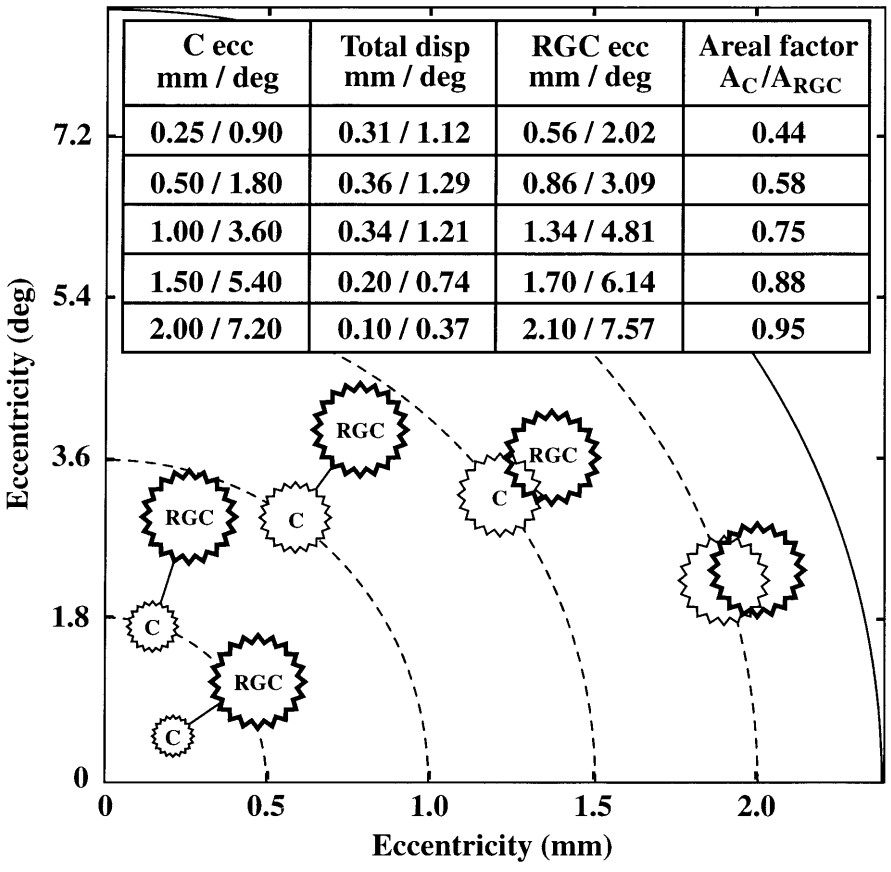

Fig. 7 A graphical presentation of the loss of visual due to disconnected cones (*C*) caused by a lesion of corresponding but displaced RGC. The lesion (RGC) area within the inner retina was held constant and the C area was varied according to the inverse areal magnification resulting from the total displacement at different eccentricities (*ecc*)

cone convergence. By assuming that the changes in RGC:C ratio totally reflect this cone convergence outside the foveal border, it is possible to calculate the area from which one RGC receives information. This area served by one RGC, regardless of cell type, is called the estimated receptive field, the density of which can be calculated by dividing effective RGC density by the central RGC:C ratio at all eccentricities [22].

Diagrammatic representation of displacement

Figure 6 summarizes the findings of the present study. It shows a colour density distribution map of raw RGC, estimated receptive fields [22] and cones [3] versus eccentricity. A number of schematic sampling units have been drawn in the map illustrating the effects of displacement. The transformation of raw RGC density, which was the highest density at the foveal border, to estimated receptive field density using the functions in Figs. 3 and 5 creates a density distribution with a steep fall from the foveal centre towards the periphery, as is the case for the cone density.

Location of scotoma due to RGC damage

Calculations of the displacement of RGC subserving more centrally located cones allow us to estimate the location and size of a central scotoma caused by a lesion of the RGC layer within the inner retina. Figure 7 demonstrates the size and displacement of corresponding areas disconnected cones and RGC and the fact that an RGC lesion just outside or at the foveal border affects vision within the fovea where the disconnected cones are located (approximately 1 deg central to RGC lesion).

Discussion

Precise knowledge of lateral displacement from the inner segment of cone photo-receptors (the location of receptive field centres of the fovea) to the retinal ganglion cell is crucial in order to understand and interpret the foveal geometry and cellular connections within the primate fovea. The present study presents direct measurements of radial offsets caused by the cone fibres within the layer of Henle in laser-lesioned and non-lesioned fovea. Data along the vertical meridian of normal retinas clearly show that the displacement is maximal at the foveal border (2.5 deg eccentricity) and thereafter decreases out to

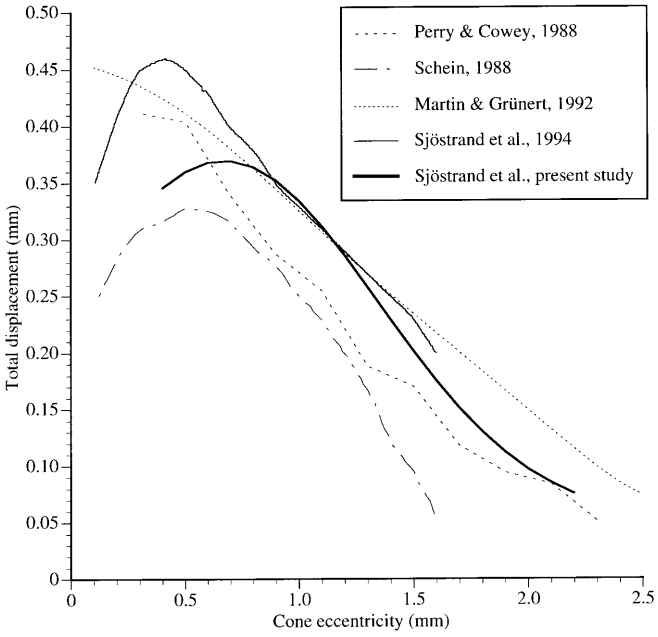

Fig. 8 Total displacement versus cone eccentricity in the human (*continuous lines*) and in the macaque (*interrupted lines*). Data from the present study is represented by the *thick continuous line* (cf. Fig. 3, Eq. III), and the *thin continuous line* represents the indirect estimate in one human case from [21]. The interrupted lines show measured total displacement in macaques (*dotted line* [14], temporal hemi-meridians; *dashed line* [17], mean of all meridians; *dash-dotted line* [20], mean of nasal and temporal hemi-meridians)

approximately 8.6 deg eccentricity. The measured displacement along the nasal hemi-meridian of one retina with laser lesions show a decline with a similar profile outside the foveal border as do displacement values along the vertical hemi-meridians. The findings of Curcio and coworkers [2, 3] of elliptical isodensity contours of cone and RGC densities make it important to further study displacement within the fovea and along the horizontal hemi-meridians outside the fovea where the present study lacks sufficient data.

On the basis of the presented measurements of displacement, it can be concluded that the RGC densities reported by Curcio and Allen [2] are too small to allow for a foveal RGC:cone ratio of 2 or greater. Conversely, the indirectly obtained displacement data extracted from RGC and cone densities and assumed RGC:cone ratios of 2 or 3 by these authors are at least 30% higher that the measurements reported in the present study. As previously discussed [1, 21] our data on RGC and cone densities obtained with the dissector differ from those of Curcio and Allen [2], who used whole-mount preparations, mainly in the thick RGC layer inside 1,5 mm eccentricity and show only minor differences at greater eccentricities or for cone densities. This may well be related to problems in resolving separate nerve cell nuclei in the whole-mount preparations due to the RGC layer thickness at the foveal border. Yet Curcio and Allen [2] claimed to have obtained similar cell densities in both sections and whole-mounts. Furthermore, it is not clearly stated in the paper by Curcio and Allen [2] whether the morphometric principles of “forbidden lines” for the counting frame were correctly used [10]. “Forbidden lines” means that objects touching two out of four edges of a measuring field should not be included in the measurements: if all objects touching the edges are included the result is an overestimate; if none of the objects touching the edges are included the result is an underestimate. This problem would affect counting in whole-mounts and sections in a similar manner.

Our human data indicate that the displacement along the vertical hemi-meridians outside 8.6 deg is of such limited extension (≤50 μm) that it hardly affects comparisons of quantitative estimates of cone and retinal ganglion cell densities. The areal chage due to 50-μm displacement at a cone eccentricity of 8.6 deg is 4% and less outside this eccentricity. Therefore, for practical purposes, the cones and their receptive field contres can be considered to be localized vertically underneath the connected RGC outside this eccentricity.

The present estimates of total displacement versus eccentricity along the vertical meridian outside the human foveal border agree well with previous indirectly estimated values [21] of total lateral displacement along the same meridian (Fig. 8). However, inside the foveal border these indirect estimates in one case were approximately 25% higher than those directly measured in the present study.

Compared with directly measured Henle fibres and estimated total displacements in macaque monkeys [14, 17] our data are of a similar magnitude outside an eccentricity of 0.6 mm (Fig. 8). Estimates of displacement within the macaque retina based on cumulative curves of cone inner segments and cone pedicle densities, together with direct measurements of stained vertical sections [20], show a similar decline outside the foveal border but yield a total displacement in the lower range of those of the macaque studies above.

Several issues concerning our estimate of total displacement have to be discussed. In the calculation of total displacement in macaque monkeys the lateral displacement caused by the dentritic trees of RGC has been estimated [17]. Since the human and macaque data show limited differences it can be assumed that displacement within the RGC layer is of a similar magnitude to that reported in macaques. To obtain the total displacement including that within the RGC layer the macaque values from [17] may be added: approximately 20 μm central to 0.5 mm, 15 μm from 0.5 to 1.0 mm and 10 μm from 1.0 to 1.6 mm eccentricity. The effect of adding RGC displacement to the caculated regression curves for the total displacement of the present study was minor. Another

problem with semithin sections in the calculation of displacement (cf. Materials and methods) is the effect of imperfect alignment of a thin cone fibre in a section. Since our criterion was that the specimen in general should be well aligned an angular deviation of less than 10 deg is anticipated. The underestimation due to this error is considered to be 1% or less. In addition it has to be further noted that our measurements of Henle fibres in 1-µm sections, in contrast to those in thick Golgi preparations, do to allow measurements of the limited distance of displacement from the inner segment of the cone photoreceptor (image plane) and the initial portion of the cone fibre to its exit from the outer nuclear layer, here defined as cone eccentricity. This underestimation, as judged from a limited number of sections, ranges from a few µm to approximately 15 µm for those cone cell bodies located deeply in the outer nuclear layer within the fovea. Furthermore, this displacement within the outer nuclear layer is varying due to the tortuous paths of the initial parts of the cone fibres. The average displacement for a cone fibre within the outer nuclear layer is estimated to be 10 µm or less. An estimate of the combined effects of all these minor underestimations from cone soma to RGC of the total displacement is of the order of 5%. Recalculations of effective RGC density and the diagrammatic representation showed that the effect of compensation for this minor underestimation was negligible. Tissue shrinkage in this study was estimated to be less than 5%. Assuming an additive effect of the possible measurement errors discussed obove and a shrinkage of 5% yields a maximum total underestimate of 10%. A recalculation of effective RGC densities with a 10% addition to the total displacement resulted in a density increase of 4% at the foveal border (0.6 mm), 3% at 0.8 mm and 1% at 1.6 mm eccentricity, none of which bear any major influence on our conclusions.

A clinically useful implication of the present study is that the locations of a scotoma following a lesion at some level of the central retina may be predictable. Lesions at the level of the pigment epithelium (also involving the photoreceptor cells) such as in laser burns (Fig. 1) will result in focal and coincident scotoma. A consequence of displaced RGC subserving centripetally located receptive fields is that lesions at the level of RGC approximately 1 deg outside the foveal border may involve loss of vision of a smaller area closer to the foveola (Fig. 7). Such lesions of the inner retina may occur when peeling epiretinal membranes during macular hole surgery. During such surgery, the internal limiting membrane of the retina together with epiretinal tissue overlying and surrounding the hole, is often removed [15, 26]. Even though no distinct retinal neural tissue is usually removed, the possibility still exists that stripping of the inner limiting membrane together with surgical trauma may induce damage to the inner retinal layers. Microperimetry might be a useful tool in ruling out the existence of such inner retinal lesions.

In conclusion, this study presents direct measurements of lateral displacement within and outside the human fovea. It shows a peak of the displacement at the foveal border and a steep decrease outside the foveal border. The presented results support and extend our previous analysis of the relation within the fovea between quantitative cell distributions and psychophysical measurements. Our data should prove useful for further analysis of the structural correlate for normal and impaired central vision, as well as for predictions of scotoma size and localization after damage to the inner retina.

Acknowledgement This study was supported by the Swedish Medical Research Council (grants 02226, 07121) and a grant from the Royal Society of Arts and Sciences in Göteborg.

References

1. Conradi N, Sjöstrand J (1993) A morphometric and stereologic analysis of ganglion cells of the central human retina. Graefe's Arch Clin Exp Ophthalmol 231:169–174
2. Curcio CA, Allen KA (1990) Topography of ganglion cells in human retina. J Comp Neurol 300:5–25
3. Curcio CA, Sloan KR, Kalina RE, Hendrickson AE (1990) Human photoreceptor topography. J Comp Neurol 292:497–523
4. Drasdo N, Fowler CW (1974) Nonlinear projection of the retinal image in a wide-angle schematic eye. Br J Ophthalmol 58:709–714
5. Eins S, Wilhelms E (1976) Assessment of preparative volume changes in central nervous tissue using automatic image analysis. Microscope 24:29–38
6. Frisen L (1995) High-pass resolution perimetry: central-field neuroretinal correlates. Vision Res 35:293–301
7. Gass JD (1988) Idiopathic senile macular hole. Its early stages and pathogenesis. Arch Ophthalmol 106:629–639
8. Gass JD (1995) Reappraisal of biomicroscopic classification of stages of development of a macular hole: (see comments) Am J Ophthalmol 119:752–759
9. Gass JD (1997) A stereoscopic atlas of macular disease, 4th edn. Mosby, St Louis
10. Gundersen HJ (1978) Estimators of the number of objects per area unbiased by edge effects. Microsc Acta 81:107–117
11. Hee MR, Izatt JA, Swanson EA, Huang D, Schuman JS, Lin CP, Puliafito CA, Fujimoto JG (1995) Optical coherence tomography of the human retina. Arch Ophthalmol 113:325–332
12. Hendrickson A, Kupfer C (1976) The histogenesis of the fovea in the macaque monkey. Invest Ophthalmol Vis Sci 15:746–756
13. MarshallJ, Hamilton AM, Bird AC (1975) Histopathology of ruby and argon laser lesions in monkey and human retina. A comparative study. Br J Ophthalmol 59:610–630

14. Martin PR, Grunert U (1992) Spatial density and immunoreactivity of bipolar cells in the macaque monkey retina. J Comp Neurol 323:269–287
15. Messmer EM, Heidenkummer HP, Kampik A (1998) Ultrastructure of epiretinal membranes associated with macular holes. Greafe's Arch Clin Exp Ophthalmol 236:248–254
16. Packer O, Hendrickson AE, Curcio CA (1990) Development redistribution of photoreceptors across the *Macaca nemestrina* (pigtail macaque) retina. J Comp Neurol 298:472–493
17. Perry VH, Cowey A (1988) The lenghts of the fibres of Henle in the retina of macaque monkeys: implications for vision. Neuroscience 25:225–236
18. Polyak S (1941) Structure of the vertebrate retina. In: Heinrick Klüver (ed) The vertebrate visual system. The University of Chicago Press, Chicago, pp 260–275
19. Puliafito CA, Hee MR, Lin CP, Reichel E, Schuman JS, Duker JS, Izatt JA, Swanson EA, Fujimoto JG (1995) Imaging of macular diseases with optical coherence tomography. Ophthalmology 102:217–229
20. Schein JS (1988) Anatomy of macaque fovea and spatial densities of neurons in foveal representation. J Comp Neurol 269:479–505
21. Sjöstrand J, Conradi N, Klaren L (1994) How many ganglion cells are there to a foveal cone? A stereologic analysis of the quantitative relationship between cone and ganglion cells in one normal human fovea. Graefe's Arch Clin Exp Ophthalmol 232:432–437
22. Sjöstrand J, Ollson V, Popovic Z, Conradi N (1999) Quantitative estimations of foveal and extra-foveal retinal circuitry in humans. Vision Res 39:2987–2998
23. Swanson EA, Hee MR, Huang D, et al (1993) In vivo retinal imaging by optical coherence tomography. Optics Lett 18:1864–1866
24. Wässle H, Grünert U, Röhrenbeck J, Boycott BB (1990) Retinal ganglion cell density and cortical magnification factor in the primate. Vision Res 30:1897–1911
25. Wyatt HJ (1992) A hypothesis concerning the relationship between retinotopy in the optic nerve head and perimetry. Clin Vision Sci 7:153–161
26. Yoon HS, Brooks HL Jr, Capone A Jr, L'Hernault NL, Grossniklaus HE (1996) Ultrastructural features of tissue removed during idiopathic macular hole surgery. (see comments) Am J Ophthalmol 122:67–75
27. Yuodelis C, Hendrickson A (1986) A qualitative and quantitative analysis of the human fovea during development. Vision Res 26:847–855